

## Frequency-Domain Analysis of the Fixed-Phase Reset Control System

Zhang, Xinxin; Hsu, Hsing Li; Hosseinnia, S. Hassan

DO

10.1109/CCTA60707.2024.10666550

Publication date

**Document Version**Final published version

Published in

Proceedings of the IEEE Conference on Control Technology and Applications, CCTA 2024

Citation (APA)

Zhang, X., Hsu, H. L., & Hosseinnia, S. H. (2024). Frequency-Domain Analysis of the Fixed-Phase Reset Control System. In *Proceedings of the IEEE Conference on Control Technology and Applications, CCTA 2024* (pp. 288-293). IEEE. https://doi.org/10.1109/CCTA60707.2024.10666550

#### Important note

To cite this publication, please use the final published version (if applicable). Please check the document version above.

Copyright

Other than for strictly personal use, it is not permitted to download, forward or distribute the text or part of it, without the consent of the author(s) and/or copyright holder(s), unless the work is under an open content license such as Creative Commons.

Takedown policy

Please contact us and provide details if you believe this document breaches copyrights. We will remove access to the work immediately and investigate your claim.

# Green Open Access added to TU Delft Institutional Repository 'You share, we take care!' - Taverne project

https://www.openaccess.nl/en/you-share-we-take-care

Otherwise as indicated in the copyright section: the publisher is the copyright holder of this work and the author uses the Dutch legislation to make this work public.

# Frequency-Domain Analysis of the Fixed-Phase Reset Control System

Xinxin Zhang, Hsing-Li Hsu, and S. Hassan HosseinNia\*

Abstract—Current reset elements mainly rely on the traditional zero-crossing resetting mechanism. This study introduces a reset element with a new resetting mechanism that distributes multiple resets within a single period for reset controllers with sinusoidal reference inputs. This new control element is termed "Fixed-Phase Reset Control (FPRC)". A higher-order sinusoidal input describing function is developed to analyze the frequency-domain properties of the new controller. The accuracy of this frequency-domain analytical approach is validated through simulations on three systems. Through the analysis, the new FPRC demonstrates phase lead compared to zero-crossing reset control, but it introduces nonlinearities at low frequencies.

#### I. Introduction

The mechatronics industry places a substantial emphasis on attaining precise positioning and high-speed performance in its systems, necessitating the optimization of controllers [1]. Linear controllers, such as Proportional-Integral-Derivative (PID) controllers, are extensively employed in industrial settings due to their effectiveness and ease of tuning. However, their performance is constrained by the inherent linear limitations outlined in Bode's phase-gain relationship [2]. In the quest for alternatives, reset control has emerged as a promising approach to surmount these linear limitations.

The pioneering work of Clegg in the 1950s introduced the simplest form of a reset controller, known as the Clegg Integrator (CI) [3]. Notably, the first-order harmonic of the CI exhibits a 52-degree phase lead while maintaining the same slope (-20 dB/decade) as the linear integrator. This characteristic challenges Bode's phase-gain relationship and shows potential for enhancing control system performance. To expand the applicability of reset control, Horowitz introduced the first-order reset element (FORE) [4], [5]. The FORE has demonstrated promising outcomes in mitigating high-frequency noise. Ongoing research in the realm of reset control has yielded various reset controller variants, as exemplified by works such as [6], [7], [8], [9]. Most preceding reset elements operate on the classical "Zero-crossing Law" resetting mechanism, where the reset controller's output resets to zero upon crossing zero by the input signal.

#### \* Corresponding Author

Xinxin Zhang is with the Department of Precision and Microsystems Engineering (PME), Delft University of Technology, Mekelweg 2, Delft, The Netherlands X.Zhang-15@tudelft.nl

Hsing-Li Hsu was with the Department of Precision and Microsystems Engineering (PME), Delft University of Technology, Mekelweg 2, Delft, The Netherlands, when he participated in this work peterhsu0507@gmail.com

S. Hassan HosseinNia is with the Department of Precision and Microsystems Engineering (PME), Delft University of Technology, Mekelweg 2, Delft, The Netherlands S.H.HosseinNiaKani@tudelft.nl

Research efforts have explored the different resetting mechanisms. Studies such as [10], [11] demonstrate that manipulating the timing of reset actions can enhance the performance of systems like PZT positioning stages. Other research indicates that pre-defining reset conditions can optimize a reset adaptive observer [12] and improve tracking capabilities in hard disk drive systems [13]. Despite these efforts, the application of the new resetting mechanism to reset controllers remains unclear. Furthermore, for the effective implementation of the new reset controller, there is a need for a frequency-domain analysis method. To the best of the authors' knowledge, there are currently no available tools for analyzing the frequency responses of reset controllers that utilize non-zero-crossing resetting mechanisms.

This study aims to overcome these limitations, and its structure is outlined as follows. Section II provides an introduction to the traditional reset control system employing the zero-crossing resetting law, encompassing its state space representation and frequency domain analysis method. Subsequently, the three primary contributions of this research are presented as follows:

- 1) In Section III, we introduce a novel reset controller termed as "Fixed-Phase Reset Control (FPRC)". The FPRC incorporates an innovative resetting mechanism that enables the reset controller's output to reset to a predefined value when a specified phase-based signal crosses zero. This mechanism is applied to common reset elements, including the CI, the FORE, and the Second-Order Single-State Reset Element (SOSRE)
- 2) Section IV formulates a Higher-Order Sinusoidal Input Describing Function (HOSIDF) for analyzing the frequency response of the Single-Input-Single-Output (SISO) FPRC under sinusoidal inputs. The accuracy of the HOSIDF for FPRC is validated through simulation. This HOSIDF method enables the analysis of the frequency domain properties of the open-loop FPRC.
- In Section V, The HOSIDF analysis shows the superior phase lead of the FPRC compared to zero-crossing reset control, but it introduces nonlinearities at low frequencies.

Finally, Section VI delivers the conclusions of this study and delineates potential avenues for future research.

## II. BACKGROUND

### A. The Definition of the Traditional Reset Controller

The closed-loop reset control system's block diagram is illustrated in Fig. 1. This system consists of various

components: a reset controller labeled as  $\mathcal{C}$ , a linear controller denoted as  $\mathcal{C}_{\alpha}$ , a plant represented as  $\mathcal{P}$ , a reference signal given by r(t), an error signal denoted as e(t), a reset output signal designated as v(t), a control input signal marked as u(t), and a measured output tracked as y(t).

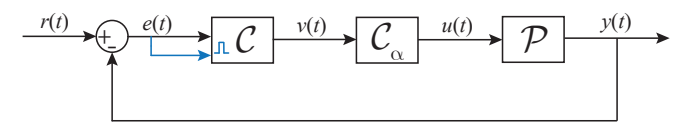


Fig. 1: The block diagram of a closed-loop reset control system, where the blue lines represent the reset action.

The state-space equations of the reset controller C with the classical "Zero-crossing Law" is expressed as follows:

$$C = \begin{cases} \dot{x}_r(t) = A_R x_r(t) + B_R e(t), & e(t) \neq 0, \\ x_r(t^+) = A_\rho x_r(t), & e(t) = 0, \\ v(t) = C_R x_r(t) + D_R e(t), \end{cases}$$
(1)

where  $x_r(t) \in \mathbb{R}^{\zeta_c}$  represents the state of the reset controller and  $\zeta_c$  is the number of states. Matrices  $A_R, B_R, C_R, D_R$  collectively define the base-linear controller (BLC) of  $\mathcal{C}$ . The transfer function of the BLC, denoted as  $\mathcal{C}_{bl}$ , is expressed as:

$$C_{bl}(\omega) = C_R (j\omega I - A_R)^{-1} B_R + D_R.$$
 (2)

The reset matrix  $A_{\rho}$  in the second equation in (1) is defined as:

$$A_{\rho} = \begin{bmatrix} \Gamma_{\zeta_r} & \\ & I_{\zeta_l} \end{bmatrix}, \Gamma_{\zeta_r} = \operatorname{diag}(\gamma_1, \gamma_1, ..., \gamma_i, ..., \gamma_{\zeta_r}), \quad (3)$$

where  $\gamma_i \in (-1,1)$ . Here,  $\zeta_r$  denotes the number of reset states,  $\zeta_l$  represents the number of linear states, and the total number of states is given by  $\zeta_c = \zeta_l + \zeta_r$ . When  $\Gamma_{\zeta_r} = I_{\zeta_r}$ ,  $\mathcal C$  represents the BLC  $\mathcal C_{bl}$ . Substituting the reset controller  $\mathcal C$  in Fig. 1 with its base-linear counterpart  $\mathcal C_{bl}$  results in the system being referred to as the base-linear system (BLS).

## B. Frequency Response Analysis of the Reset Controller

Let  $V(\omega)$  and  $E(\omega)$  represent the Fourier transforms of the output v(t) and input  $e(t) = |E|\sin(\omega t + \angle E)$  signals of the reset controller  $\mathcal C$ . These signals exhibit n harmonics in  $V(\omega)$  and  $E(\omega)$ , denoted as  $V_n(\omega)$  and  $E_n(\omega)$ . The transfer function of  $\mathcal C$  denoted as  $H_n(\omega)$  incorporates n harmonics, as expressed in [14], [15] and given by

$$\begin{split} H_n(\omega) &= \frac{V_n(\omega)}{E_n(\omega)} = \\ \begin{cases} C_R(j\omega I - A_R)^{-1}(I + j\Theta_D(\omega))B_R + D_R, & \text{for } n = 1, \\ C_R(jn\omega I - A_R)^{-1}j\Theta_D(\omega)B_R, & \text{for odd } n > 1, \\ 0, & \text{for even } n \geqslant 2, \end{cases} \end{split}$$

with

$$\Lambda(\omega) = \omega^{2} I + A_{R}^{2}, 
\Delta(\omega) = I + e^{(\frac{\pi}{\omega}A_{R})}, 
\Delta_{r}(\omega) = I + A_{\rho}e^{(\frac{\pi}{\omega}A_{R})}, 
\Gamma_{r}(\omega) = \Delta_{r}^{-1}(\omega)A_{\rho}\Delta(\omega)\Lambda^{-1}(\omega), 
\Theta_{D}(\omega) = \frac{-2\omega^{2}}{\pi}\Delta(\omega)[\Gamma_{r}(\omega) - \Lambda^{-1}(\omega)].$$
(5)

# III. NEW RESET ELEMENT: FIXED-PHASE RESET CONTROL

#### A. The Definition of the Fixed-Phase Reset Control

We introduce a novel reset element termed Fixed-Phase Reset Control (FPRC). This reset mechanism involves multiple resets within a single steady-state period, evenly spaced in terms of phase. Our emphasis in this paper is on the SISO FPRC system, specifically designed for sinusoidal inputs.

**Definition 1.** The state-space representation for the FPRC, denoted as  $\widetilde{C}$ , under a sinusoidal input signal  $e(t) = |E|\sin(\omega t)$  is given by:

$$\widetilde{C} = \begin{cases}
\dot{x}_r(t) = A_R x_r(t) + B_R e(t), & t \notin U, \\
x_r(t^+) = A_\rho x_r(t), & t \in U, \\
v(t) = C_R x_r(t) + D_R e(t).
\end{cases}$$
(6)

The set of reset instants  $U=\{t_i=\frac{2\pi i}{\omega k},\ i\in\mathbb{N}\}$  is an unbounded time sequence increasing monotonously with respect to  $i\in\mathbb{N}$ , i.e.,  $t_i< t_{i+1}$  for any  $i\in\mathbb{N}$  and  $\lim_{i\to\infty}=+\infty$ . In traditional reset controller  $\mathcal C$  defined in (1), the set of reset instants is defined as  $\{t_i\}=\{t_i|e(t_i)=0,\ t_i< t_{i+1}\}$ . However, in our new proposed reset controller  $\widetilde{\mathcal C}$ , the reset triggered signal is denoted as  $e_s=\sin(k\omega t)$ , where the variable k denotes the number of reset instants per steady-state cycle, with  $k=2h,\ h\in\mathbb Z^+$ . When k=2, the FPRC  $\widetilde{\mathcal C}$  is equivalent to the conventional reset controller  $\mathcal C$ .

Define  $\Delta_i = t_{i+1} - t_i$ . Neglecting the input r(t), research [10] established the stability condition for  $\widetilde{\mathcal{C}}$  as presented in the following proposition:

**Proposition 1.** If both  $\Delta_i = \delta$  is a constant and  $A_{\rho} \equiv M$  is a constant matrix, then the reset system  $\widetilde{C}$  in (6) with the zero initial condition  $x_r(0) = 0$  is (asymptotically) stable if and only if [10]

$$|\lambda(Me^{A_R}\delta)| \le 1, \ (<1), \ \forall \delta \in \mathbb{R}^+,$$
 (7)

where  $\lambda(\cdot)$  denotes the eigenvalue of  $(\cdot)$ .

The stability of the system and the existence of steadystate solutions are essential for proving the main results in this paper. To establish the necessary conditions, we introduce the following assumption.

**Assumption 1.** The FPRC defined in (6), is assumed to satisfy the condition specified in Proposition 1. The reset actions are assumed to be finite in any finite time. The initial condition of the reset controller is zero, i.e.,  $x_r(0) = 0$ .

In practice, the base-linear system of  $\widetilde{C}$  in (6) is usually designed to be stable. In this case, the bounded constraint on  $\{\Delta t_i\}$  can be relaxed [10].

#### B. Fixed-Phase Reset Control Elements

In this study, we integrate the novel Fixed-Phase (FP) resetting mechanism into three reset control structures: the CI, the FORE, and the SOSRE, with their state-space matrices defined as follows.

1) The state-space matrices of the CI are

$$A_R = 0$$
,  $B_R = 1$ ,  $C_R = 1$ ,  $D_R = 0$ ,  $A_\rho = \gamma$ . (8)

2) The state-space matrices of the FORE are

$$A_R = -\omega_r, \ B_R = 1, \ C_R = \omega_r, \ D_R = 0, \ A_\rho = \gamma.$$
(9)

3) The SOSRE refers to a second-order reset element that resets the first state  $x_2(t)$ , as shown in Fig. 2. The state-space matrices of SOSRE are given by:

$$A_{R} = \begin{bmatrix} -2\beta\omega_{r} & -\omega_{r}^{2} \\ 1 & 0 \end{bmatrix}, B_{R} = \begin{bmatrix} 1 \\ 0 \end{bmatrix},$$

$$C_{R} = \begin{bmatrix} 0 & \omega_{r}^{2} \end{bmatrix}, D_{R} = 0, A_{\rho} = \begin{bmatrix} \gamma & 0 \\ 0 & 1 \end{bmatrix}.$$
(10)

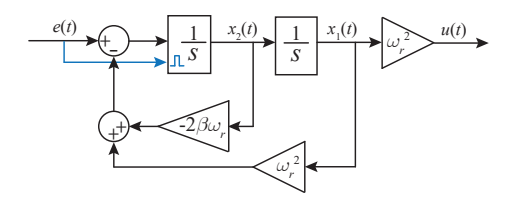


Fig. 2: The block diagram of the SOSRE.

Applying the new reset mechanism defined in (6) to the three control structures, the resulting reset control elements are termed as "Fixed-Phase CI (FP-CI)", "Fixed-Phase FORE (FP-FORE)", and "Fixed-Phase SOSRE (FP-SOSRE)".

#### IV. THE FREQUENCY-DOMAIN ANALYSIS OF THE FPRC

#### A. The Open-loop HOSIDF for FPRC systems

Due to the nonlinearity of the FPRC, the reset output signal v(t) is characterized by an infinite series of harmonics, defined as  $v(t) = \sum_{n=1}^{\infty} v_n(t)$ . In the Fourier domain, it is expressed as  $V(\omega) = \sum_{n=1}^{\infty} V_n(\omega)$ . As illustrated in Fig. 3, to generate  $v_n(t)$ , we employ the "Virtual Harmonics Generator" [16] to produce harmonics  $e_n(t)$  from the input  $e(t) = |E|\sin(\omega t)$ , expressed as:

$$e_n(t) = |E|\sin(n\omega t), n \in \mathbb{Z}^+.$$
 (11)

Define  $E(\omega)$  and  $E_n(\omega)$  as the Fourier transforms of e(t) and  $e_n(t)$ , respectively.

**Theorem 1.** The Higher-Order Sinusoidal Input Describing Function (HOSIDF) for the FPRC system in (6) with a sinusoidal input  $e(t) = |E|\sin(\omega t)$  and a reset triggered

signal  $e_s(t) = \sin(k\omega t)(k=2h, h \in \mathbb{Z}^+)$ , under Assumption 1, is denoted as  $\widetilde{H}_n(\omega)$ . It is defined to describe the transfer function from the input  $e_n(t)$  to the output  $v_n(t)$ . The expression for  $\widetilde{H}_n(\omega)$  is as follows:

$$\widetilde{H}_{n}(\omega) = \frac{V_{n}(\omega)}{E_{n}(\omega)} = \begin{cases} \mathcal{C}_{bl}(\omega) + \widetilde{\Phi}(\omega), & \text{for } n = 1, \\ \widetilde{\Phi}(n\omega), & \text{for odd } n > 1, \\ 0, & \text{for even } n \geq 2, \end{cases}$$
(12)

with

$$\widetilde{\Phi}(n\omega) = \frac{2}{n\pi|E|} \Delta_l(n\omega) \widetilde{\Theta}(n\omega),$$

$$\Delta_l(n\omega) = C_R(jn\omega I - A_R)^{-1} jn\omega I,$$

$$\widetilde{\Theta}(n\omega) = (\gamma - 1) \sum_{i=1}^{\frac{k}{2} - 1} m_i e^{j\frac{2n\pi i}{k}},$$
(13)

where  $m_0 = 0$  and  $m_i$  (where  $i \in \mathbb{Z}^+$ ) for  $\widetilde{C}$  with different state numbers  $\zeta_c$  are provided as follows.

1) For the FR-CI and FR-FORE with  $\zeta_c = 1$ ,

$$m_i = m_{i-1}e^{A_R t_i} + [B_R e^{A_R t} * e(t)]|_{t_i}.$$
 (14)

2) For the FR-SOSRE with  $\zeta_c = 2$ ,

$$m_{i} = \mathcal{L}^{-1}[\Omega_{i}(s)/s]|_{t_{i-1}},$$

$$\Omega_{i+1}(s) = \frac{E(s) + (s + 2\beta\omega_{r})\mathcal{L}^{-1}[\Omega_{i}(s)]|_{t_{i}}}{s^{2} + 2\beta\omega_{r}s + \omega_{r}^{2}}.$$
(15)

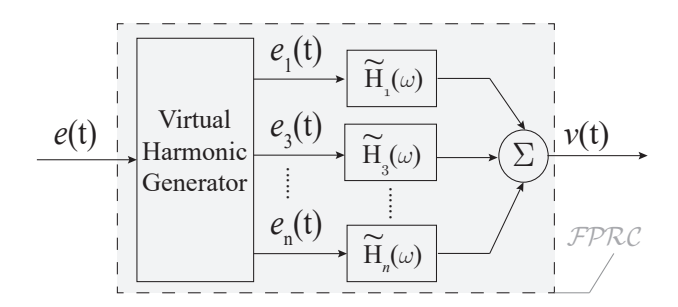


Fig. 3: The HOSIDF for FPRC systems.

*Proof.* The proof is divided into scenarios with  $\zeta_c=1$  for the FP-CI and FP-FORE, and with  $\zeta_c=2$  for the FP-SOSRE. Note that the FP-CI is identical to the FP-FORE when  $\omega_r=0$  in (9). When  $\zeta_c=1$ ,  $m_i$  is set to  $x_r(t_i)$ . When  $\zeta_c=2$  for the FP-SOSRE,  $x_r(t)=[x_2(t)\ x_1(t)]^T$ . In this case,  $m_i=x_2(t_i)$ . We set  $m_0=0$  due to the zero-initial condition of the reset controller. Here, we first present the scenario with  $\zeta_c=1$ .

Between two reset instants  $(t_i, t_{i+1}]$ , the FPRC experiences no reset. It can be seen as the base-linear system with an initial condition inherent from the time interval  $(t_{i-1}, t_i]$ . From (6), during  $(t_i, t_{i+1}]$ , we have

$$\dot{x}_r(t) = A_R x_r(t) + B_R e(t). \tag{16}$$

The Laplace transform of (16) is given by

$$sX_r(s) - x_r(t_{i-1}) = A_R X_r(s) + B_R E(s) \Leftrightarrow X_r(s) = (s - A_R)^{-1} (x_r(t_i) + B_R E(s)),$$
(17)

where  $x_r(t_i)$  is the initial condition of  $x_r(t)$  for  $t \in (t_i, t_{i+1}]$ . The inverse Laplace transform of (17) is given by

$$x_r(t) = x_r(t_i)e^{A_R t} + [B_R e^{A_R t} * e(t)](t).$$
 (18)

From (18), the state  $x_r(t)$  at the reset instant  $t_{i+1}$  can be derived as follows:

$$x_r(t_{i+1}) = x_r(t_i)e^{A_R t_i} + [B_R e^{A_R t} * e(t)]|_{t_{i+1}}.$$
 (19)

From (19), for the FPRC with  $\zeta_c = 1$  and  $m_i = x_r(t_i)$ , we have

$$m_i = m_{i-1}e^{A_R t_i} + [B_R e^{A_R t} * e(t)]|_{t_i}.$$
 (20)

This concludes the  $m_i$  for the FP-CI and FP-FORE with  $\zeta_c=1$ .

From (6), at  $t_i = 2\pi i/(\omega k)$ , the reset action introduces a pulse signal into the  $x_r(t)$ , given by

$$\Omega_i = x_r(t_i^+) - x_r(t_i) = (A_\rho - I)x_r(t_i). \tag{21}$$

When  $\zeta_c = 1$ ,  $A_\rho = \gamma$ .

Substituting  $m_i = x_r(t_i)$  into (21), we have

$$\Omega_i = x_r(t_i^+) - x_r(t_i) = (\gamma - 1)m_i.$$
 (22)

Equation (22) indicates that the reset action introduces a pulse signal  $\Omega_i$  to the state  $x_r(t)$ . Since the periodic property of the base-linear and reset output, the reset actions in the time domain introduce a square wave denoted as q(t) with an amplitude of  $(\gamma-1)m_i/2$ , a period of  $2\pi/\omega$ , and a phase shift of  $i2\pi/k$  to  $x_1(t)$ , which can be seen as a disturbance [17]. Define a normalized square wave with an amplitude of 1 and a period of  $2\pi/\omega$ , and a phase shift of 0 as  $q_0(t)$  given by

$$q_0(t) = \frac{4}{\pi} \sum_{n=1}^{\infty} \frac{\sin(\omega t)}{n}.$$
 (23)

The Fourier transform of  $q_0(t)$ , denoted as  $Q_0(\omega)$ , is given by:

$$Q_0(\omega) = \frac{4}{\pi} \sum_{n=1}^{\infty} \frac{E(n\omega)}{n|E|}.$$
 (24)

Thus, q(t) and its Fourier transform are given by

$$q(t) = \mathcal{F}^{-1}[Q(\omega)],$$

$$Q(\omega) = \frac{(\gamma - 1)}{2|E|} \sum_{i=1}^{\frac{k}{2} - 1} m_i e^{j\frac{2n\pi i}{k}} Q_0(\omega).$$
(25)

From (24) and (25), the *n*-th harmonic in  $Q(\omega)$  defined as  $Q_n(\omega)$  is given by

$$Q(\omega) = \sum_{n=1}^{\infty} Q_n(\omega),$$

$$Q_n(\omega) = \frac{2(\gamma - 1)}{\pi |E|} \sum_{i=1}^{\frac{k}{2} - 1} \frac{m_i e^{j\frac{2n\pi i}{k}} E(n\omega)}{n}.$$
(26)

From (6), the transfer function from the  $x_r(t)$  to v(t) is defined as

$$\Delta_I(\omega) = C_R (i\omega I - A_R)^{-1} i\omega I. \tag{27}$$

Taken consider the q(t) as a disturbance adding to the  $x_r(t)$ , the reset output signal v(t) is given by

$$v(t) = v_{bl}(t) + v_{nl}(t),$$

$$v_{bl}(t) = \mathscr{F}^{-1}[\mathcal{C}_{bl}(\omega)E(\omega)],$$

$$v_{nl}(t) = \mathscr{F}^{-1}[\Delta_{l}(\omega)Q(\omega)].$$
(28)

From (24), (26), and (28),  $V_{nl}(\omega) = \mathscr{F}^{-1}[v_{nl}(t)]$  is given by

$$V_{nl}(\omega) = \sum_{n=1}^{\infty} \frac{2(\gamma - 1)\Delta_l(n\omega)}{n\pi |E|} \sum_{i=1}^{\frac{k}{2}-1} m_i e^{j\frac{2n\pi i}{k}} E(n\omega).$$
(29)

Define  $V_{nl}^n(\omega)$  as the *n*-th harmonic in  $V_{nl}(\omega)$ . From (29), we have

$$V_{nl}(\omega) = \sum_{n=1}^{\infty} V_{nl}^{n}(\omega),$$

$$V_{nl}^{n}(\omega) = \frac{2(\gamma - 1)\Delta_{l}(n\omega)}{n\pi|E|} \sum_{i=1}^{\frac{k}{2}-1} m_{i}e^{j\frac{2n\pi i}{k}} E(n\omega).$$
(30)

Based on (28) and (30), the first-order harmonic in  $V(\omega) = \mathscr{F}[v(t)]$  is obtained as

$$V_1(\omega) = V_{bl}(\omega) + V_{nl}^1(\omega). \tag{31}$$

From (28) and (31), the first-order (n = 1) transfer function of FPRC is defined as

$$\widetilde{H}_{1}(\omega) = \frac{V_{1}(\omega)}{E(\omega)}$$

$$= C_{bl}(\omega) + \frac{2(\gamma - 1)\Delta_{l}(\omega)}{\pi |E|} \sum_{i=1}^{\frac{k}{2}-1} m_{i} e^{j\frac{2n\pi i}{k}}.$$
(32)

From (28) and (30), the  $n\text{-th}\ (n>1)$  order harmonic in  $V(\omega)$  is given by

$$V_n(\omega) = V_{nl}^n(\omega). \tag{33}$$

Then, based on (33), the n-th transfer function of FPRC is defined as

$$\widetilde{H}_n(\omega) = \frac{V_n(\omega)}{E(n\omega)} = \frac{2(\gamma - 1)\Delta_l(n\omega)}{n\pi|E|} \sum_{i=1}^{\frac{k}{2}-1} m_i e^{j\frac{2n\pi i}{k}}.$$
(34)

By defining  $\widetilde{\Phi}(n\omega)$  and  $\widetilde{\Theta}_n(n\omega)$  in (13), equation (12) is obtained. Here The proof for the FPRC with  $\zeta_c=1$  is concluded. The following content derives  $m_i$  for the FP-SOSRE with  $\zeta_c=2$ .

In FP-SOSRE, we have  $x_r(t) = [x_2(t) \ x_1(t)]^T$ , where  $x_2(t)$  and  $x_1(t)$  denote the first and the second state of the controller, respectively, as shown in Fig. 2. From (6) and (10), during the time interval  $(t_i, t_{i+1}]$ , the state-space representation of FP-SOSRE can be written as follows:

$$\begin{cases} \dot{x}_1(t) = x_2(t), \\ \dot{x}_2(t) = -2\beta\omega_r x_2(t) - \omega_r^2 x_1(t) + e(t). \end{cases}$$
(35)

The Laplace transforms of both sides from Equation (35) with the inital condition of  $x_1(t_i)$  are given by

$$s^{2}X_{1}(s) - sx_{1}(t_{i}) = -2\beta\omega_{r}(sX_{1}(s) - x_{1}(t_{i})) - \omega_{r}^{2}X_{1}(s) + E(s).$$
(36)

From (36),  $X_1(s)$  is obtained as

$$X_1(s) = \frac{E(s) + (s + 2\beta\omega_r)x_1(t_i)}{s^2 + 2\beta\omega_r s + \omega_r^2}.$$
 (37)

By conducting the inverse Laplace transform of (37), we have

$$x_1(t) = \mathcal{L}^{-1} \left\{ \frac{E(s) + (s + 2\beta\omega_r)x_1(t_i)}{s^2 + 2\beta\omega_r s + \omega_r^2} \right\}, \text{ for } t \in (t_i, t_{i+1}].$$
(38)

Define

$$\Omega_{i}(s) = \frac{E(s) + (s + 2\beta\omega_{r})x_{1}(t_{i})}{s^{2} + 2\beta\omega_{r}s + \omega_{r}^{2}}.$$
(39)

Substituting  $\Omega_i(s)$  into (38),  $x_1(t)$  is given by

$$x_1(t) = \mathcal{L}^{-1}[\Omega_i(s)], \text{ for } t \in (t_i, t_{i+1}].$$
 (40)

From (38),  $x_1(t_{i+1})$  is given by

$$x_1(t_{i+1}) = \mathcal{L}^{-1}[\Omega_i(s)]|_{t_i}. (41)$$

Based on (39) and (41), we have

$$\Omega_{i+1}(s) = \frac{E(s) + (s + 2\beta\omega_r)\mathcal{L}^{-1}[\Omega_i(s)]|_{t_i}}{s^2 + 2\beta\omega_r s + \omega_r^2}.$$
 (42)

From (40) and  $\dot{x_1}(t) = x_2(t)$ ,  $x_2(t)$  is given by

$$x_2(t) = \mathcal{L}^{-1}[\Omega_i(s)/s], \text{ for } t \in (t_i, t_{i+1}].$$
 (43)

From (43),  $x_2(t_{i+1})$  is given by

$$x_2(t_{i+1}) = \mathcal{L}^{-1}[\Omega_i(s)/s]|_{t_i}.$$
 (44)

Since  $m_i = x_2(t_i)$ , from (44),  $m_i$  is given by

$$m_i = \mathcal{L}^{-1}[\Omega_i(s)/s]|_{t_{i-1}}.$$
 (45)

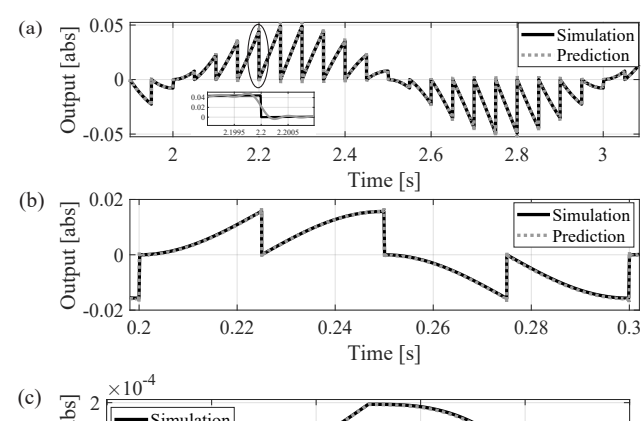
This completes the derivation of  $m_i$  for the FP-SOSRE with  $\zeta_c = 2$ . The subsequent steps for deriving  $\widetilde{H}_n(\omega)$  for the FP-SOSRE follow the same process as the derivations from (23) to (34). Here, we conclude the proof.

In practical scenarios, the system in (6) with a sinusoidal input  $e(t) = |E|\sin(\omega t)$  and under Assumption 1 will initially undergo a transient response before reaching the steady-state. The frequency response analysis in Theorem 1 is applicable to systems at steady-states. Therefore, we calculate  $m_i$  until the cycle has a reset instant  $t_i$  meeting the condition of  $m_i = m_{i+k}$ . This cycle is denoted as the first valid steady-state cycle.

#### V. RESULTS

# A. Illustrative Example 1: Validation of the Accuracy of the HOSIDF

We verify the accuracy of the HOSIDF method in Theorem 1 by applying it to analyze three FPRC examples. Figures 4(a)-(c) depict the simulated and predicted outputs of three FPRC systems under the input signal  $e(t) = \sin(2\pi ft)$ , including the FP-CI (with  $\gamma=0$  and k=20) at an input frequency of f=1 Hz, the FP-FORE (with  $\omega_r=1$ ,  $\gamma=0$ , and k=4) at an input frequency of f=10 Hz, and the FP-SOSRE (with  $\omega_r=1$ ,  $\beta=1$ ,  $\gamma=0$ , and k=4) at an input frequency of f=10 Hz. The results indicate a



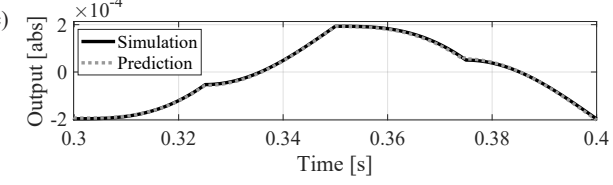


Fig. 4: The simulated and Theorem 1-predicted outputs for (a) the FP-CI, (b) the FP-FORE, and (c) the FP-SOSRE.

close alignment between the predicted and simulated outputs, confirming the accuracy of Theorem 1.

The small differences between the simulation and prediction results stem from the fact that the output of the reset system includes an infinite number of harmonics, whereas in practice, only a finite number (set to 1000 in Fig. 4) of harmonics is considered in the calculation. Figure 5 illustrates the prediction error (PE) between the prediction and simulation in the context of the FP-CI shown in Fig. 4(a). It shows that as the number of harmonics  $N_h$  increases, the PE decreases. Ideally, the PE approaches zero as  $N_h$  tends to infinity. Research [18] also demonstrates that the accuracy of the HOSIDF analysis improves as  $N_h$ , the number of harmonics considered in the analysis, increases.

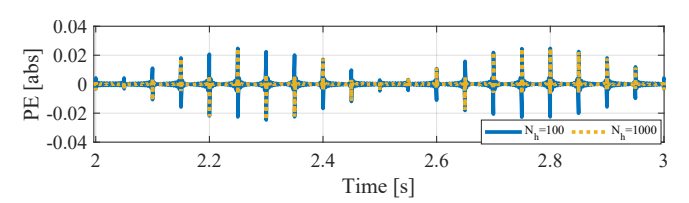


Fig. 5: The prediction error (PE) of the FP-CI when (a)  $N_h = 100$  and (b)  $N_h = 1000$ .

# B. Illustrative Example 2: Frequency-domain Properties of the FPRC

We employ the HOSIDF analysis to investigate the frequency-domain properties of the FPRC. The reset control system (RCS) employing the FPRC is referred to as FP-RCS and the reset system employing the "Zero-crossing (ZC) law" is denoted as ZC-RCS.

Figure 6(a) compares the frequency responses of the FP-CI (with k=4 and  $\gamma=0$ ) and the traditional ZC-CI (with k=2 and  $\gamma=0$ ). Their gain-frequency (slope) is the same,

but the first-order harmonic in FP-CI provides an 8.4° phase lead compared to that of the CI.

Figure 6(b) illustrates the relationship between the number of reset instants k and the phase of the FP-CI (with  $\gamma=0$ ). As the number of reset instants increases, the phase lead provided by the FP-CI also increases. This characteristic of the FP-CI demonstrates the potential benefits for improved performance achieved by the phase lead of the FPRC.

However, a large number of reset instants k will generate higher-order harmonics. As shown in Fig. 6(c), when setting k = 20, the three dominant harmonics in the FP-CI are the first, 19th, and 21st harmonics. Although it eliminates the 3rd and 5th harmonics, it introduces higher-order harmonics.

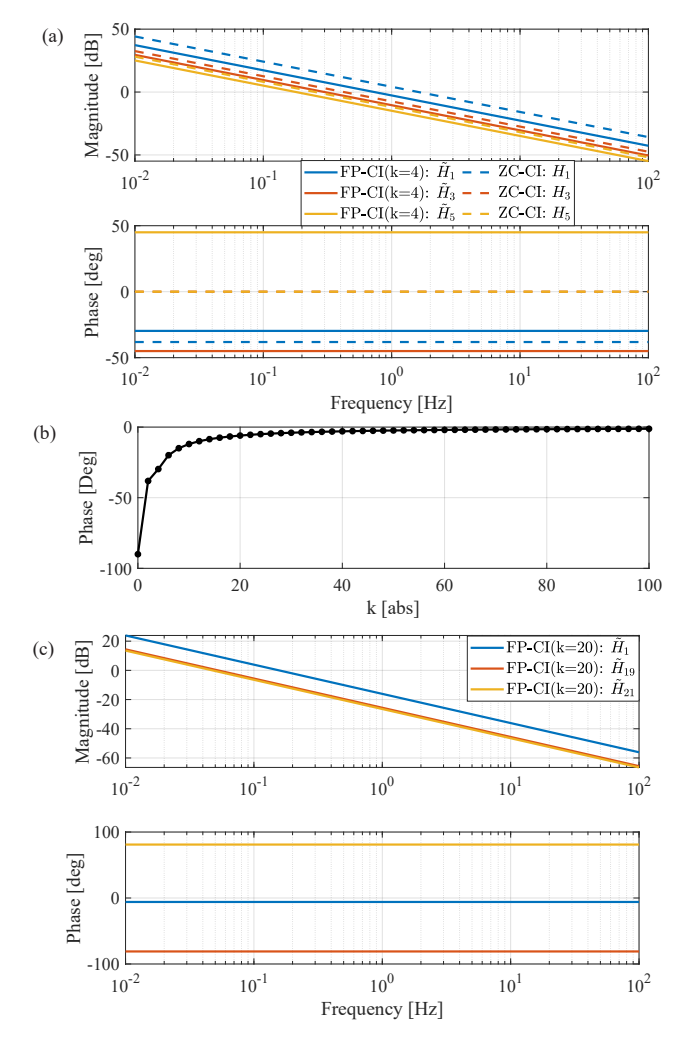


Fig. 6: (a) The first three dominant harmonics in the FP-CI (with k=4) and the ZC-CI. (b) The relationship between the phase of the first-order harmonic and the number of reset instants k in the FP-CI. (c) The first three dominant harmonics in the FP-CI (with k=20).

#### VI. CONCLUSION

This paper introduces a novel reset element termed Fixed-Phase Reset Control (FPRC), designed for Single-Input-Single-Output (SISO) systems with sinusoidal inputs. The

FPRC resets based on a signal with a fixed phase, distributing k reset instants per steady-state period. A Higher-Order Sinusoidal Input Describing Function (HOSIDF) is developed to analyze the frequency-domain properties of the FPRC. Simulation results validate the accuracy of the analysis method. The findings indicate that the FPRC provides a phase lead compared to traditional reset controllers with the zero-crossing law. Increasing the value of k tends to provide a larger phase benefit; however, higher values of k introduce high-order harmonics into the system. The applicability of the FPRC with the phase benefits to practical closed-loop systems needs further investigation in future studies.

#### REFERENCES

- [1] Kok Kiong Tan, Tong Heng Lee, and Sunan Huang. *Precision motion control: design and implementation*. Springer Science & Business Media, 2007.
- [2] Karl Åström and Richard Murray. Feedback Systems: An Introduction for Scientists and Engineers. Princeton University Press, 2010.
- [3] J. C. Clegg. A nonlinear integrator for servomechanisms. Transactions of the American Institute of Electrical Engineers, Part II: Applications and Industry, 77:41–42, 1958.
- [4] Isaac Horowitz and Patrick Rosenbaum. Non-linear design for cost of feedback reduction in systems with large parameter uncertainty. *International Journal of Control*, 21(6):977–1001, 1975.
- [5] K. R. Krishnan and I. M. Horowitz. Synthesis of a non-linear feedback system with significant plant-ignorance for prescribed system tolerances. *International Journal of Control*, 19(4):689–706, 1974.
- [6] Alfonso Banos and Angel Vidal. Definition and tuning of a pi+ ci reset controller. In 2007 European Control Conference (ECC), pages 4792–4798 IEEE 2007
- [7] Leroy Hazeleger, Marcel Heertjes, and Henk Nijmeijer. Second-order reset elements for stage control design. In 2016 American Control Conference (ACC), pages 2643–2648. IEEE, 2016.
- [8] Niranjan Saikumar and Hassan HosseinNia. Generalized fractional order reset element (gfrore). In 9th European Nonlinear Dynamics Conference (ENOC), 2017.
- [9] N. Saikumar, R. K. Sinha, and S. H. HosseinNia. constant in gain lead in phase" element–application in precision motion control. *IEEE/ASME Transactions on Mechatronics*, 24:1176–1185, 2019.
- [10] M. F. Y. W. J. Zheng, Y. Guo, and L. Xie. Improved reset control design for a pzt positioning stage. In 2007 IEEE International Conference on Control Applications, 2007.
- [11] D. Paesa, J. Carrasco, O. Lucia, and C. Sagues. On the design of reset systems with unstable base: A fixed reset-time approach. In *IECON* 2011 - 37th Annual Conference of the *IEEE Industrial Electronics* Society, pages 646–651, 2011.
- [12] D. Paesa, A. Baños, and C. Sagues. Optimal reset adaptive observer design. Systems and Control Letters, 60(10):877–883, 2011.
- [13] Y. Guo, Y. Wang, L. Xie, H. Li, and W. Gui. Optimal reset law design of reset control systems with application to hdd systems. In Proceedings of the 48h IEEE Conference on Decision and Control (CDC) held jointly with 2009 28th Chinese Control Conference, pages 5287–5292, 2009.
- [14] A. A. Dastjerdi, A. Astolfi, N. Saikumar, N. Karbasizadeh, D. Valério, and S. H. HosseinNia. Closed-loop frequency analysis of reset control systems. arXiv preprint arXiv:2001.10487, 2020.
- [15] Kars Heinen. Frequency analysis of reset systems containing a clegg integrator: An introduction to higher order sinusoidal input describing functions. 2018.
- [16] Niranjan Saikumar, Kars Heinen, and S. Hassan HosseinNia. Loop-shaping for reset control systems: A higher-order sinusoidal-input describing functions approach. Control Engineering Practice, 111:104808, 2021.
- [17] Marcin B. Kaczmarek, Xinxin Zhang, and S. Hassan HosseinNia. Steady-state nonlinearity of open-loop reset systems. In 2022 IEEE Conference on Control Technology and Applications (CCTA), pages 1056–1060. IEEE, 2022.
- [18] Xinxin Zhang, Marcin B. Kaczmarek, and S. Hassan HosseinNia. Frequency-domain analysis for reset systems using pulse-based model. arXiv preprint arXiv:2206.00523, 2022.